Effect of Proline Content and Histidine Ligation on the Dynamics of Ω-Loop D and the Peroxidase Activity of Iso-1-cytochrome *c*

William J. Martin,[a,d] Levi J. McClelland,[a,b,c,] Shiloh M. Nold,[a] Kassandra L. Boshae,[a] and Bruce E. Bowler[a,c,]*

[a] Department of Chemistry & Biochemistry, University of Montana, Missoula, Montana 59812, United States

[b] Division of Biological Sciences, University of Montana, Missoula, Montana, 59812, United States

[c] Center for Biomolecular Structure & Dynamics, University of Montana, Missoula, Montana 59812, United States

[d] Present address: European Vaccine Initiative, Universitäts Klinikum Heidelberg, Vossstrasse 2, Geb. 4040, 69115 Heidelberg, Germany

*To whom correspondence should be addressed.

Telephone: (406) 243-6114. Fax: (406) 243-4227. E-mail: bruce.bowler@umontana.edu

ABSTRACT:

To study how proline residues affect the dynamics of Ω-loop D (residues 70 to 85) of cytochrome *c*, we prepared G83P and G83A variants of yeast iso-1-cytochrome *c* (iso-1-Cyt*c*) in the presence and absence of a K73H mutation. Ω-loop D is important in controlling both the electron transfer function of Cyt*c* and the peroxidase activity of Cyt*c* used in apoptosis because it provides the Met80 heme ligand. The G83P and G83A mutations have no effect on the global stability of iso-1-Cyt*c* in presence or absence of the K73H mutation. However, both mutations destabilize the His73-mediated alkaline conformer relative to the native state. pH jump stopped-flow experiments show that the dynamics of the His73-mediated alkaline transition are significantly enhanced by the G83P mutation. Gated electron transfer studies show that the enhanced dynamics result from an increased rate of return to the native state, whereas the rate of loss of Met80 ligation is unchanged by the G83P mutation. Thus, the G83P substitution does not stiffen the conformation of the native state. Because bis-His heme ligation occurs when Cyt*c* binds to cardiolipin-containing membranes, we studied the effect of His73 ligation on the peroxidase activity of Cyt*c*, which acts as an early signal in apoptosis by causing oxygenation of cardiolipin. We find that the His73 alkaline conformer suppresses the peroxidase activity of Cyt*c*. Thus, the bis-His ligated state of Cyt*c* formed upon binding to cardiolipin is a negative effector for the peroxidase activity of Cyt*c* early in apoptosis.

Key Words: Cytochrome *c*, Protein dynamics, Peroxidase activity, Conformationally-gated electron transfer, Alkaline conformational transition, Apoptosis

1. Introduction

Proline is unique among the set of monomers used to make proteins in nature in that it is an imino acid [1]. The imino acid results from the side chain of proline forming a five-membered ring with the α-amino group, constraining the ϕ dihedral angle to be near -60°. When incorporated into proteins, the probability that an X-Pro peptide bond adopts a cis conformation is higher than for other peptide bonds. The unusual conformational properties of proline lead to a preference for proline in turn structures [2], and at the N1 position of helices [3]. These conformational preferences have led to the "Proline Rule" for stabilizing proteins which states that: "A globular protein can be additively thermostabilized by increasing the frequency of proline occurrence in the second positions of β-turns (and in the N1 positions of α-helices or on coils) on the surface of the molecule without major changes in the functional and structural integrity, in such a way that the folded state becomes less flexible while the unfolded state is further reduced in the backbone conformational entropy" [4]. The approach has proved broadly effective in a wide range of proteins [5-7]. The conformational constraints on proline stiffen the protein backbone. One measure of the stiffening of the backbone imposed by proline is the significantly increased persistence length of polyproline sequences relative to other amino acid homopolymers [8,9]. This stiffening of the protein backbone in the native state is thought to stabilize native protein structure by locking it in place. However, as noted above proline also constrains the conformational entropy of the unfolded state, destabilizing it relative to the native state [7].

Recently, there has been considerable interest in how protein function can be mediated by transiently populated alternate conformers of proteins [10]. In considering the use of proline to favor a conformer, it is important to consider the effect of proline on both conformers. While

proline can stabilize turns and the N1 position of helices, it is considered a helix breaker because the peptide bond involving an imino NH lacks the necessary amide NH to form intrahelical hydrogen bonds [1]. A two-proline variant of the Sars-CoV-2 spike protein (S-2P) is the primary component of most vaccines used to protect against Sars-CoV-2 infection [11]. In the Sars-CoV-2 spike protein, a helix-turn-helix motif in the highly antigenic prefusion conformer becomes part of a helical coiled-coil structure in the postfusion conformer [11]. In S-2P, the two prolines are introduced into the turn segment of the prefusion conformer and act to stabilize the prefusion state by destabilizing the helical postfusion conformer [11-13]. We recently developed a tool for rational stabilization of proteins, EmCAST [14], which indicates that the proline substitutions in S-2P have a small stabilizing effect on the pre-fusion conformer, but substantially destabilize the post-fusion conformer.

For heme proteins used in biological electron transfer reactions, the stiff backbone enforced by prolines could assist in minimizing the reorganization energy associated with redox reactions thereby increasing the rates of long-range electron transfer in proteins. For mitochondrial cytochrome *c* (Cyt*c*), the degree of preference for the native ligation of the heme is also important for controlling access to alternate conformers that are associated with peroxidase activity. In the intrinsic pathway of apoptosis, oxygenation of cardiolipin by the peroxidase activity of Cyt*c* is used as an early signal [15].

The axial ligands of *c*-type heme electron transfer (ET) proteins typically are located in surface loops [16]. For *c*-type hemes with a methionine axial ligand, the loop containing this ligand is often rich in proline and glycine side chains (Fig. 1). The Pro/Gly content ranges from about one third in the 15 residue loop containing Met80 in mitochondrial Cyt*c* [16,17] to about two thirds of the residues in the short 9 residue loop containing Met71 in cytochrome c_{553} from

Bacillus pasteurii [18-21]. For bacterial *c*-type cytochromes (cytochromes c_8), such as *Pseudomonas aeruginosa* and *P. Stutzeri* cytochrome c_{551}, the Met ligand to the heme (Met61) is part of a loop with a rigid polyproline helix (prolines at positions 58, 61, 62 and 63) [22,23]. Both NMR relaxation and hydrogen-deuterium exchange methods show that this Pro-rich loop is unusually rigid compared to mitochondrial cytochromes *c* [22,24]. Counterintuitively, this rigidity can induce strain that in some cases promotes fluxional behavior [25,26].

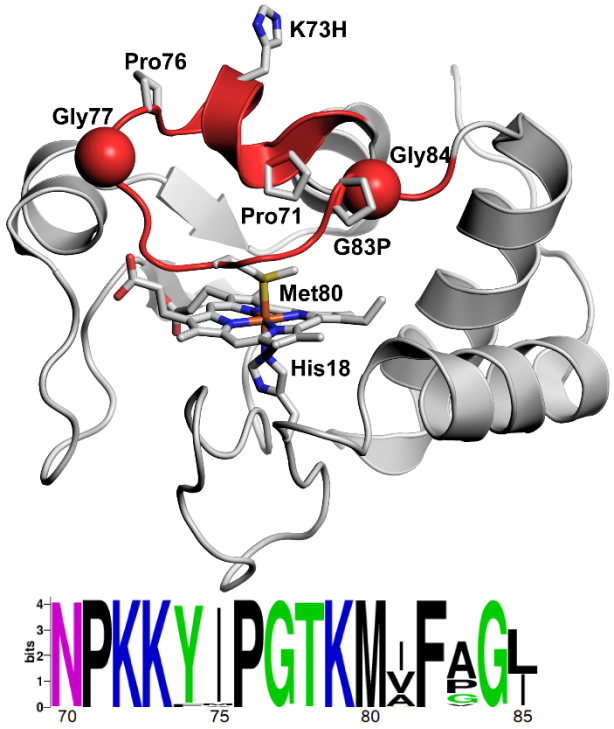

Fig. 1. Structure of K73H/G83P iso-1-Cyt*c*. The heme and its ligands, Met80 and His18, are shown as stick models colored by element. Ω-loop D is shown in red with prolines shown as stick models and glycines shown as spheres. The K73H and G83P mutations are shown as stick models. The mutations were introduced into the structure of oxidized yeast iso-1-Cyt*c* (pdb file: 2YCC[27]) using the mutagenesis function of PyMol [28]. The sequence logo at the bottom of the figure was produced with WebLogo [29] using the sequence alignment in Banci *et al* [17].

Ω-loop D (residues 70 – 85) of mitochondrial Cyt*c* (Fig. 1) is longer than the surface loops of either *B. pasteurii* Cytc_{553} or the Cytc_8 family proteins. It has been speculated that the increased length of this loop is responsible for the increased dynamics of mitochondrial Cyt*c* relative to its bacterial counterparts and that the increased dynamics may be adaptive for recognizing various

redox partners [24,25]. Ω-loop D is highly conserved [17] (see Fig. 1); it contains two conserved prolines (Pro71 and Pro76) and two conserved glycines (Gly77 and Gly84). Position 81, which evolves from Ala → Val → Ile in eukaryotes [30], and position 83, which is Gly in lower eukaryotes and Val in primates, are the most variable residues in this loop (Fig. 1). The human V83G variant has been well studied [31,32] as has the G83V variant in yeast iso-1-Cyt*c* [33]. Both the human V83G and the yeast G83V variants increase the pK_a of the alkaline transition. The forward rate constant for the alkaline transition is smaller for both variants suggesting that in their individual sequence context both stabilize the native relative to the alkaline conformer of the protein. At position 83, Ala and Pro are also common in mitochondrial Cyt*c* (Fig. 1). Substitution of Gly83 of yeast iso-1-Cyt*c* with proline (Fig. 1) thus provides a good opportunity to evaluate the effects of a proline residue on the stability and dynamics of Cyt*c*. The dynamics of Ω-loop D are closely linked to the dynamics of the alkaline transition of Cyt*c* [34,35]. We have also substituted Lys73 with a histidine so that we can more readily monitor the dynamics of the alkaline transition as mediated by the residue at position 73. For comparison with the effect of proline at position 83 on the dynamics of Ω-loop D, we also study the G83A variant. Furthermore, to relate the effects of proline on the dynamics of Cyt*c* to the function of Cyt*c*, we have evaluated the peroxidase activity of these variants of iso-1-Cyt*c*, to shed light on how Pro mutations modulate this activity, which is important in the early stages of apoptosis [15].

2. Experimental section

2.1. Preparation of iso-1-Cytc variants carrying mutations at positions 73 and 83

All variants of iso-1-Cyt*c* were prepared in the pRbs_BTR1 vector [36]. In this vector, an optimized Shine-Dalgarno sequence from *Escherichia coli* [37] replaces the ribosomal binding

site from the gene 10 leader sequence of phage T7 used in the pBTR1 vector [38]. The pRbs_BTR1 also expresses yeast heme lyase (*CYC3*), so that heme can be attached covalently to Cyt*c* in *Escherichia coli* [39]. pRbs_BTR1 carrying either the WT* iso-1-Cyt*c* gene or WT* with a K73H mutation was used as template for PCR-based mutagenesis (QuikChange, Agilent Technologies). The WT* iso-1-Cyt*c* gene contains a C102S mutation (eliminates dimerization during physical studies) [40] and a K72A mutation. Lys72 is trimethylated when iso-1-Cyt*c* is expressed in *Saccharomyces cerevisiae*, so, the K72A mutation stops formation of a Lys72-heme alkaline conformer [39]. The sequences of the primers used to introduce the G83A and G83P mutations are given in Table S1. The sequences of the G83A, K73H/G83A, G83P and K73H/G83P variants in the WT* background were confirmed by dideoxy sequencing (University of Montana Genomics Core).

2.2. Growth and purification of iso-1-Cytc variants

All variants were expressed from *E. coli* BL21(DE3) cells (EdgeBio, Gaithersburg, MD) as described previously [41]. In brief, a freshly transformed plate of *E. coli* cells was suspended in 3 mL of sterile L-broth and used to inoculate 1 L of 2xYT media (2.8 L Fernbach flask). After 18 hrs in a shaker incubator (125 rpm) at 37 ºC, cells were harvested (10 min at 5,000 rpm; GS-3 rotor; Sorvall RC 5C+, 4 ºC). Pellets were stored at -80 ºC. Three freeze (-80 ºC)/thaw (4 ºC) cycles were used in advance of lysis using a French Press. The lysis buffer was 50 mM Tris, pH 8, 500 mM NaCl, 1 mM EDTA (2 mL/g of cell paste). Small amounts of DNase I and RNase A were added as well as PMSF (2 mM final concentration to inhibit proteolysis).

Purification of the cleared lysate included removal of impurities by 50% ammonium sulfate saturation followed by cation exchange chromatography (CM Sepharose) as described previously

[41]. Iso-1-Cyt*c* variants were concentrated by ultrafiltration after chromatography, flash frozen in liquid nitrogen, and stored at -80 ºC.

Immediately prior to experiments, iso-1-Cyt*c* variants were thawed and purified to homogeneity by HPLC (Agilent 1200; BioRad UNO S6 column) using previously described methods [41]. Ultrafiltration was used to concentrate the purified variants and exchange them into 50 mM sodium phosphate, pH 7.

Iso-1-Cyt*c* variants were oxidized with $K_3[Fe(CN)_6]$, as described previously [42], followed by Sephadex G-25 size exclusion chromatography to remove excess $K_3[Fe(CN)_6]$ and to exchange the variant into the buffer needed for the experiment.

2.3. Global stability assessed by guanidine hydrochloride titrations

Guanidine hydrochloride (GdnHCl) mediated denaturation of all iso-1-Cyt*c* variants was monitored using an Applied Photophysics Chirascan circular dichroism (CD) spectrometer interfaced to a Hamilton MICROLAB 500 titrator, as described previously [35,43]. Ellipticity at 222 nm, θ_{222}, and 250 nm, θ_{250}, was recorded at each GdnHCl concentration. A 20 mM Tris, pH 7.5, 40 mM NaCl buffer was used. A two-state model assuming a linear relationship between the free energy of unfolding, ΔG_u, and GdnHCl concentration was fit to plots of $\theta_{222corr} = \theta_{222} - \theta_{250}$ versus GdnHCl concentration [44]. There is often curvature in the native baseline of GdnHCl titrations of iso-1-Cyt*c* caused by binding of Cl^- at low GdnHCl concentration [45]. As a result, this part of the native baseline was not used in the fits to the data and the native state baseline was assumed to be independent of GdnHCl concentration [46].

2.4. Alkaline conformational transition of iso-1-Cytc variants

The alkaline conformation transition in which a lysine or histidine from Ω-loop D replaces Met80 as the heme ligand was monitored at 695 nm using a Beckman DU800 UV-Vis spectrometer for the WT*G83A, WT*K73H/G83A, WT*G83P and WT*K73H/G83P variants, using previously described pH titration procedures [41-43]. This absorbance band reports on the presence of Met80-heme ligation [16]. Absorbance at 750 nm, A_{750}, was used to correct for baseline drift during experiments. Titrations were carried out in the presence of 0.1 M NaCl at 22 ± 1 °C. For the G83A and G83P variants, eq.1, a modified form of the Henderson-Hasselbalch equation that accounts of the number of protons linked to the alkaline conformational transition, was fit to plots of $A_{695corr} = A_{695} - A_{750}$ versus pH. In eq. 1, A_{Alk} is the corrected absorbance at

$$(1)\quad A_{695\mathrm{corr}} = \frac{A_{\mathrm{Alk}} + A_{\mathrm{N}} \times 10^{n[\mathrm{pH}_{1/2} - \mathrm{pH}]}}{1 + 10^{n[\mathrm{pH}_{1/2} - \mathrm{pH}]}}$$

695 nm of the alkaline state, A_N is the corrected absorbance at 695 nm of the native state, $pH_{1/2}$ is the midpoint pH and *n* is the number of protons linked to the alkaline transition.

For variants containing His73, the alkaline transition has two phases. The first phase involves His73-heme ligation and typically does not completely replace Met80 [47]. In the second phase, Lys79 replaces both Met80 and His73 (Fig. 2).

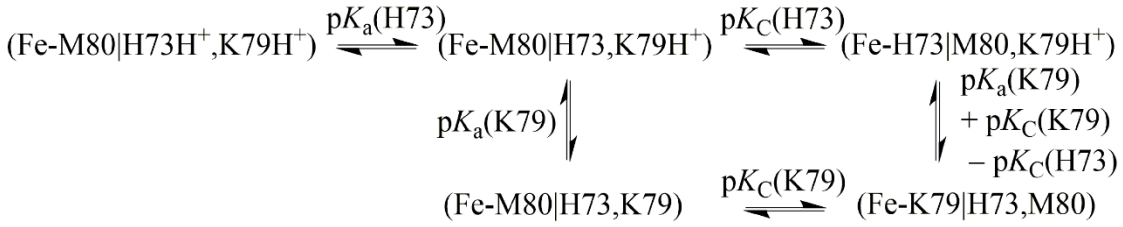

Fig. 2. Alkaline transition for variants containing His73.

This model yields eqs. 2 and 3 for the dependence of $A_{695corr}$ on pH,

$$(2)\quad A_{695\mathrm{corr}} = \frac{A_{\mathrm{N}} + A_{\mathrm{Alk}} \times K_{\mathrm{obs}}}{1 + K_{\mathrm{obs}}}$$

$$(3)\ K_{\mathrm{obs}} = \frac{K_{\mathrm{C}}(\mathrm{H73})}{1+\left(\frac{[\mathrm{H^+}]}{K_{\mathrm{a}}(\mathrm{H73})}\right)} + \frac{K_{\mathrm{C}}(\mathrm{K79})}{1+\left(\frac{[\mathrm{H^+}]}{K_{\mathrm{a}}(\mathrm{K79})}\right)} = \frac{10^{-\mathrm{p}K_{\mathrm{C}}(\mathrm{H73})}}{1+10^{(\mathrm{p}K_{\mathrm{a}}(\mathrm{H73})-\mathrm{pH})}} + \frac{10^{-\mathrm{p}K_{\mathrm{C}}(\mathrm{K79})}}{1+10^{(\mathrm{p}K_{\mathrm{a}}(\mathrm{K79})-\mathrm{pH})}}$$

In these equations, K_{obs} is the observed equilibrium constant as a function of H^+ concentration (pH), K_a(H73) and pK_a(H73) represent the acid dissociation constant of the group that triggers the His73-mediated alkaline transition and its pK_a, K_a(K79) and pK_a(K79) represent the acid dissociation constant of the group that triggers the Lys79-mediated alkaline transition and its pK_a, K_C(H73) and pK_C(K79) are the conformational equilibrium constant between the deprotonated form of Cyt*c* and the His73 alkaline conformer and its pK_C (-log*K*c) and K_C(K79) and pK_C(K79) are the conformational equilibrium constant between the deprotonated form of Cyt*c* and the Lys79 alkaline conformer and its pK_C.

2.5. pH jump stopped-flow measurements

Oxidized WT*K73H, WT*K73H/G83A or WT*K73H/G83P iso-1-Cyt*c* in 0.1 M NaCl was adjusted to a pH near 5. Upward pH jump experiments were accomplished by 1:1 mixing of the 0.1 M NaCl solution of iso-1-Cyt*c* at ~ pH 5 with 20 mM buffers containing 0.1 M NaCl to achieve final pH values from ~6.5 to ~ 10.25 in increments of 0.25 pH units. Mixing was accomplished at 25 ºC with an Applied Photophysics SX20 stopped-flow spectrometer (Leatherhead, UK). Buffers were: pH 6.5: MES buffer; pH 6.75-7.5, phosphate buffer; pH 7.75-8.75, Tris buffer; pH 9.0-10.0, boric acid buffer; pH 10.25, CAPS buffer. After mixing, the buffer concentration was 10 mM with 0.1 M NaCl and the protein concentration was 10 μM. Absorbance was monitored at 406 nm. Each pH jump was monitored first for one run at 100-650 seconds, to determine the length of time necessary for the alkaline transition. Then, five mixes were done for the appropriate time span, followed by ten 1 s runs that monitored specifically the His 73-mediated alkaline transition. For downward pH jump experiments, the 0.1 M NaCl

solution of the K73H variant was adjusted to pH 8. For downward pH jumps, the 20 mM buffers were: sodium acetate (pH 5.00, 5.25); MES, sodium salt (pH 5.50, 5.75, 6.00, 6.25 and 6.50). Exponential equations were used to fit the data using SigmaPlot (v. 13) to extract rate constants and amplitudes.

2.6. Gated electron transfer studies

Conformationally-gated electron transfer (gated ET) measurements were carried out as previously described [42,48-50] using hexaaminеruthenium(II) chloride as the reducing agent. Briefly, 10 mM sodium phosphate, pH 7, 0.1 M NaCl was degassed using a dual vacuum/inert gas manifold (multiple cycles of vacuum followed by refilling with argon). The degassed buffer was used to purge the flow system of an Applied Photophysics SX20 stopped-flow spectrometer immediately prior to use. After oxidation of the WT*K73H/G83P variant to the Fe(III) state as described above, the variant was diluted into degassed 10 mM sodium phosphate, pH 7, 0.1 M NaCl to a concentration of 10 μM, followed by at least 3 cycles of vacuum/refilling with argon. Solid hexaaminеruthenium(II) chloride was dissolved directly into degassed 10 mM sodium phosphate, pH 7, 0.1 M NaCl to produce concentrations of approximately 2.5, 5, 10 and 20 mM hexaaminеruthenium(II) chloride followed by at least 3 cycles of vacuum/refilling with argon. The exact concentration of the hexaaminеruthenium(II) chloride solution was evaluated by UV-Vis spectroscopy, as described previously [48]. Iso-1-Cyt*c* and hexaaminеruthenium(II) chloride solutions were transferred to the stopped-flow using gas-tight syringes followed by 1:1 mixing. Reduction of iso-1-Cyt*c* as a function of time was monitored at 550 nm. Exponential functions were fit to the data to extract rate constants for reduction of iso-1-Cyt*c* by direct and gated ET.

2.7. Peroxidase activity measurements

Peroxidase activity of iso-1-Cyt*c* variants were measured by converting guaiacol to tetraguaiacol [51,52], in the presence of H_2O_2. Tetraguaiacol produces a strong absorbance at 470 nm. Yeast iso-1-Cyt*c* variants were oxidized with potassium ferricyanide, $K_3[Fe(CN_6)]$, at room temperature for 7 to 10 minutes. The $K_3[Fe(CN_6)]$ was then separated from the protein using a G25 Sephadex desalting column with 50 mM sodium phosphate buffer at pH 7 or in 50 mM tris(hydroxymethyl)aminomethane (Tris) at pH 8 as the elution buffer. The buffers were degassed under argon for 30 to 45 minutes to limit oxidation of guaiacol by O_2. Solutions of 4 μM protein, 400 μM guaiacol, and 100 ± 6 mM hydrogen peroxide were made in the degassed buffers. The H_2O_2 concentration used was selected so that it was above the Michaelis constant, K_m, of H_2O_2 for peroxidase activity (~37 mM for human Cyt*c*) [53,54]. Guaiacol and H_2O_2 concentrations were measured by absorbance using ε_{274}= 2150 $M^{-1}cm^{-1}$ [55], and ε_{240}= 41.5 $M^{-1}cm^{-1}$ [56,57], respectively. The protein solution, degassed buffer, and variable volumes of guaiacol solution were mixed together immediately prior to measurements. Each final protein/guaiacol solution was then mixed with the 100 mM H_2O_2 solution in a 1:1 ratio using an Applied Photophysics SX20 stopped-flow spectrometer. Time-dependent changes were measured and recorded at 470 nm (A_{470}). The final concentration of protein was 1 μM, the final H_2O_2 concentration was 50 mM with a buffer concentration of 50 mM. All measurements were at 25 ± 0.1 °C. Five kinetic traces were recorded for each concentration of guaiacol. A_{470} was plotted as a function of time for each trial, and the highest slope of the linear region following the lag phase was used to determine the initial enzyme velocity, *v*. The slopes were averaged, then multiplied by 4 (oxidation of guaiacol removes 4 electrons [51,52]), divided by the protein concentration and the reported extinction coefficient [51,52] of 26.6 $M^{-1}cm^{-1}$ for tetraguaiacol

(3,3'-dimethoxy-4,4'-biphenoquinone, [58]) yielding v/[Cyt*c*] values as a function of guaiacol concentration. The catalytic rate constant, k_{cat}, and the Michaelis constant, K_m, were extracted by fitting the Michaelis-Menten equation to plots of v/[Cyt*c*] versus guaiacol concentration. The statistical significance of differences in the obtained parameters was evaluated with a two-tailed t-test. Parameters were considered to be significantly different if $p < .05$. The p-values are reported in the text.

3. Results

3.1. Global and local stability of G83P and G83A variants

The G83A and G83P were made in the presence and absence of a K73H mutation. The K73H mutation has the advantage that it shifts the alkaline conformational transition of iso-1-Cyt*c* mediated by a heme ligand at position 73 to lower pH [35,47]. In this manner, the effects of the G83A and G83P mutations on local unfolding due to formation of the His73-heme alkaline conformer can be determined with high accuracy [35].

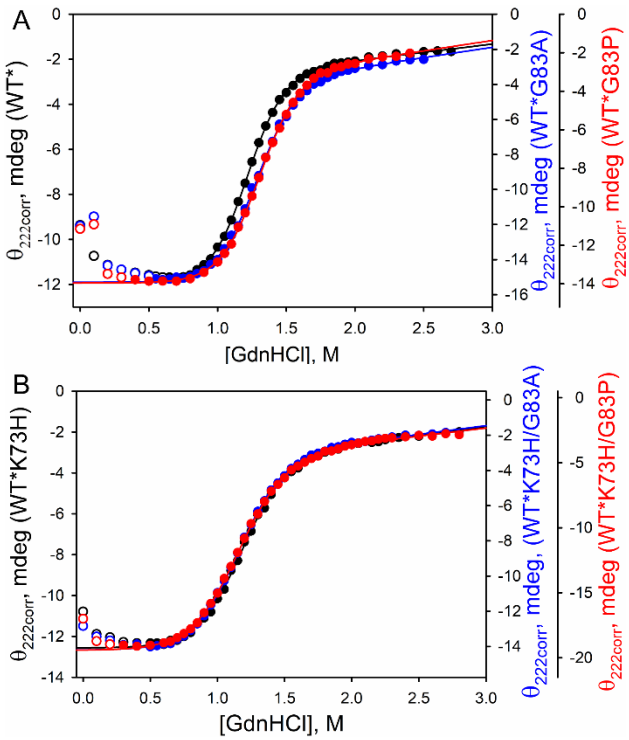

Fig. 3. GdnHCl denaturation monitored by circular dichroism at 25 °C and pH 7.5 for G83A and G83P variants in the (A) WT* and (B) WT*/K73H backgrounds. The WT* and WT*/K73H data are reproduced from previously published data [48] to allow comparison with the current results. Fits (solid lines) to the data assume two-state folding and a linear free energy relationship.

The global unfolding of the G83A and G83P variants in the presence and absence of the K73H mutation are compared to previous published data [48] for WT* and WT*/K73H in Fig. 3. The G83A and G83P mutations (Fig. 3A) both shift the denaturation midpoint, C_m, to larger values. However, the net effect on stability extrapolated to zero denaturant concentration, $\Delta G_u^{o\prime}(H_2O)$, is minor due to a decrease in the denaturant *m*-value, which is proportional to the change in solvent accessibility for the denatured state versus the native state of a protein [59], for these variants (Table 1). In the presence of the K73H mutation (Fig. 3B), the G83A and G83P mutations have no apparent effect on the GdnHCl unfolding curves and yield similar values of $\Delta G_u^{o\prime}(H_2O)$ as observed for the WT*/K73H variant. As is typical of variants containing the K73H mutation, the *m*-value is significantly decreased relative to variants in the WT*

background. Our previous studies show that the decrease in the *m*-value results from partial unfolding caused by replacement of Met80 by His73 as the heme ligand [60]. GdnHCl unfolding monitored by CD at 222 nm does not detect the partial unfolding of Ω-loop D induced by replacement of Met80 by His73 [60], which precedes global unfolding detected by CD spectroscopy at higher GdnHCl concentrations during the equilibrium unfolding titration.

Table 1
Thermodynamic parameters for iso-1-Cyt*c* variants obtained by GdnHCl denaturation monitored by CD at 25 °C and pH 7.5.

Variant [a]	$\Delta G_u^{o'}(H_2O)$ (kcal/mol)	*m*-value (kcal $mol^{-1}M^{-1}$)	C_m (M)
WT*	5.31 ± 0.08	4.39 ± 0.09	1.21 ± 0.01
WT*G83A	5.25 ± 0.02	4.06 ± 0.03	1.29 ± 0.01
WT*G83P	5.39 ± 0.13	4.13 ± 0.10	1.31 ± 0.01
WT*K73H	4.09 ± 0.11	3.49 ± 0.12	1.17 ± 0.01
WT*K73H/G83A	3.95 ± 0.06	3.44 ± 0.06	1.148 ± 0.006
WT*K73H/G83P	3.86 ± 0.16	3.35 ± 0.22	1.16 ± 0.03

[a] The pseudo wild type, WT*, contains a K72A mutation to prevent formation of a Lys72-heme alkaline conformer for protein expressed in *Escherichia coli*, which does not trimethylate this residue as for expression in yeast [39]. WT* also contains a C102S mutation to prevent disulfide dimerization during physical studies. Parameters for WT* and WT*K73H are from McClelland *et al* [48].

We next monitored the local stability of these variants by measuring the alkaline transition, a conformational change that occurs at mildly alkaline pH for mitochondrial cytochromes *c* and involves replacement of the Met80 heme ligand by an ionizable amino acid side chain from Ω-loop D (Fig. 4) [16,61,62]. For yeast iso-1-Cyt*c*, the Ω-loop D ligands are normally Lys73 and Lys79 [63]. However, when iso-1-Cyt*c* is expressed from *E. coli*, Lys72 is not trimethylated as in *S. cerevisiae*, and it also can act as a ligand in the alkaline state [39]. The variants used here

have a K72A mutation to eliminate this possibility. When Lys73 is replaced with His, it forms an alkaline conformer near neutral pH. However, this conformational change does not typically go to completion, allowing extraction of the pK_a of the ionizable group involved and the free energy for the conformational transition mediated by the fully ionized His73 (see Fig. 2) [35,47].

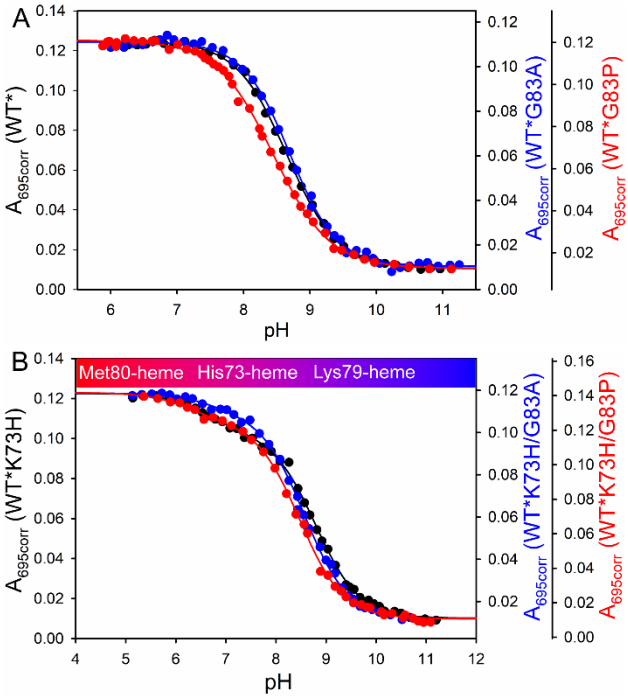

Fig. 4. Alkaline conformational transition of the G83A and G83P variants in the (A) WT* and (B) WT*K73H backgrounds. Absorbance at 695, $A_{695corr}$, was monitored versus pH to observe loss of Met80 ligation. Data were collected in the presence of 0.1 M NaCl at 22 ± 1 °C.

All studies on the alkaline transition were carried out in the presence of 100 mM NaCl to allow ready comparison with previous data from our lab and others, which were also carried out at this ionic strength [48,63]. Previous work demonstrates that the effect of ionic strength on the midpoint of the alkaline transition saturates at or just above 100 mM NaCl [63]. The alkaline transition data for the G83A and G83P variants in the WT* background (Figure 4A) show the usual sigmoidal alkaline transition with about one proton linked to the transitions (Table 2). In the case of the G83A variant, the stability of the alkaline state relative to the native state is

unchanged compared to WT* iso-1-Cyt*c* (Fig. 4A and Table 2). However, for the G83P variant the alkaline state is slightly stabilized (by ~0.4 kcal/mol; $\Delta\Delta G_{alk} = RT\Delta pH_{1/2}$) relative to the native state compared to WT* iso-1-Cyt*c* (Fig. 4A and Table 2).

Table 2
Thermodynamic parameters for the alkaline transition of variants of iso-1-Cyt*c* in 0.1 M NaCl at 22 ºC. [a]

Variant	$pH_{1/2}$	n [b]
WT* [c]	8.65 ± 0.01	1.15 ± 0.02
WT*G83A	8.68 ± 0.04	1.18 ± 0.08
WT*G83P	8.38 ± 0.08	0.96 ± 0.06
yeast WT [d]	8.62 ± 0.01	0.92 ± 0.01

[a] Parameters are the average and standard deviation of a minimum of three trials.
[b] Number of protons linked to the alkaline transition.
[c] Parameters are from McClelland et al. [48].
[d] Contains trimethyllsine 72, parameters are from Nelson and Bowler [47].

For all variants which contain the K73H mutation, the alkaline transition is biphasic (Fig. 4B). Between pH 6 and 8, the His73-heme variant partially populates. Above pH 8, a more abrupt transition occurs as Lys79 displaces the mixture of Met80 and His73 ligation present near pH 8. For His73-containing variants, fits of the equilibrium model in Fig. 2 (eqs. 2 and 3) to the data are excellent as can be seen in Fig. 4B. The parameters obtained (Table 3) show that the His73-mediated alkaline conformer is disfavored by ~0.6 kcal/mol for the G83A mutation and by ~0.2 kcal/mol for the G83P mutation ($\Delta\Delta G_C(H73) = RT\Delta pK_C(H73)$) compared to the WT*K73H variant. By contrast, the Lys79-mediated alkaline conformer is favored by ~0.45 kcal/mol for both the G83A and G83P mutations ($\Delta\Delta G_C(K79) = RT\Delta pK_C(K79)$) compared to the WT*K73H variant (Table 3). As observed previously [35,47,48], the pK_a of the ionizable group that triggers

the His73-mediated alkaline transition, pK_a(H73), is near the value expected for the imidazole side chain of a surface-exposed histidine [64]. If the parameters in Table 3 are used to calculate the relative populations of Met-ligated, His-ligated and Lys-ligated forms for the WT*K73H, WT* K73H/G83A and WT*K73H/G83P variants as a function of pH (Fig. S1), in all cases the His-ligated form begins to populate near pH 6, reaches a maximum population near pH 7.5 then decreases in population as the more stable Lys79-ligation replaces both Met80 and His73 ligation at high pH (in all cases pK_C(K79) is at least 1.9 pK units more negative than pK_C(H73), thus Lys79 ligation will dominate at high pH).

Table 3

Thermodynamic parameters for the alkaline transition of iso-1-Cyt*c* variants containing a K73H mutation obtained in 0.1 M NaCl and at 22 ºC. [a,b]

Variant	pK_C(H73)	pK_C(K79)	pK_a(H73)
WT*K73H [c]	0.67 ± 0.04	-1.20 ± 0.05	6.70 ± 0.14
WT*K73H/G83A	1.10 ± 0.09	-1.54 ± 0.02	6.63 ± 0.10
WT*K73H/G83P	0.83 ± 0.07	-1.52 ± 0.04	6.21 ± 0.19
yeast K73H [d]	0.26 ± 0.03	-1.16 ± 0.03	6.71 ± 0.08

[a] Parameters are the average and standard deviation of a minimum of three trials.

[b] In fits of eq. 3 to the data, pK_H in Table 5 was used as pK_a(K79).

[c] Data from McClelland *et al*. [48] refit using pK_H in Table 5 as pK_a(K79) in eq. 3.

[d] Contains trimethyllsine 72, parameters are refit from data in Nelson and Bowler [47] using pK_H = 9.8 ± 0.4 from the Lys79 kinetic data in Martinez and Bowler [65].

The opposing effects on stability for alkaline states involving a ligand from position 73 appear to roughly cancel out for the G83A and G83P variants in the WT* background. When Lys72 is trimethylated (tml72), the His73 alkaline conformer is stabilized relative to the native state, however the effect on the stability of the Lys79 alkaline state appears to be minimal. This

observation suggests that $pH_{1/2}$ (Table 2) reflects the equilibrium between the native conformer and an alkaline state dominated by Lys79 ligation for both WT iso-1-Cyt*c* expressed from yeast and WT* iso-1-Cyt*c* expressed from *E. coli* (Table 2). The lower $pH_{1/2}$ for WT*G83P is consistent with this conclusion based on pK_C(K79). However, the lack of an effect on the $pH_{1/2}$ for WT*G83A suggests that this mutation may affect the preference for Lys73 versus Lys79.

*3.2. pH jump kinetics of the alkaline conformational transition of WT*K73H iso-1-Cytc variants*

The kinetics of the alkaline conformational transition of the G83A and G83P variants of WT*K73H iso-1-Cyt*c* are expected to lead to a faster phase on an ~50 ms time scale due to displacement of the Met80 heme ligand by His73 and a slower phase on an ~10 sec time scale due to Lys79 becoming the heme ligand [48,65]. To measure the dynamics of the His73-mediated alkaline transition of the WT*K73H/G83A and WT*K73H/G83P variants, we used pH jump stopped-flow kinetic methods. For both the WT*K73H/G83A and WT*K73H/G83P variants, three kinetic phases were detected in both upward and downward pH jump experiments.

Both variants had a fast phase that yielded rate constants, $k_{obs,1}$, that ranged from 10 – 25 s^{-1} (40 – 100 ms timescale), consistent with the displacement of Met80 by His73. Two slower phases produced rate constants $k_{obs,2}$ and $k_{obs,3}$ that ranged from 0.1 – 1 s^{-1} (1 – 10 s timescale) and 0.01 – 0.4 s^{-1} (2.5 – 100 s timescale), respectively (Figs. S2 and S3, Tables S2 to S5). For downward pH jumps from pH 8, the magnitude of $k_{obs,2}$ is near 0.1 s^{-1} for both variants (Tables S3 and S5) and it has a relatively constant ratio with respect to the amplitude of $k_{obs,1}$ (A_{2d}/A_{1d} = 0.25 ± 0.05 for the WT*K73H/G83P variant and A_{2d}/A_{1d} = 0.27 ± 0.06 for the WT*K73H/G83A variant, where A_{1d} and A_{2d} are the amplitudes of downward pH jumps for the $k_{obs,1}$ and $k_{obs,2}$ phases, respectively). The time scale of this phase is consistent with proline isomerization. The

nearly constant A_{2d}/A_{1d} ratio suggested that this phase is a proline isomerization phase linked to the His73-heme alkaline conformer as has been observed previously [65]. For upward pH jump experiments, $k_{obs,2}$ is also near 0.1 s^{-1} up to pH 8.68 ($A_{2u}/A_{1u} = 0.25 \pm 0.03$, where A_{1u} and A_{2u} are the amplitudes of upward pH jumps for the $k_{obs,1}$ and $k_{obs,2}$ phases, respectively) for the WT*K73H/G83A variant, consistent with this interpretation (Table S4). In upward pH jump experiments, we had difficulty detecting the $k_{obs,2}$ phase below pH 8.2 for the WT*K73H/G83P variant. At higher pH, $k_{obs,2}$ increases in magnitude as does its amplitude (Tables S2 and S4). In this pH regime, $k_{obs,2}$ and $k_{obs,3}$ approach each other in magnitude, such that the value of $k_{obs,2}$ and its amplitude may be less reliable. However, we cannot rule out the possibility that other processes that effect the heme environment begin to compete with the proline isomerization phase above pH 8.6. For both variants, the magnitude of $k_{obs,3}$, increases significantly above pH 8 as does its amplitude (Tables S2 and S4). By pH 9 it is the dominant phase. This behavior is consistent with Lys79 displacing Met80 (or His73) as the heme ligand and becoming the dominant alkaline state ligand above pH 8 as seen in the equilibrium alkaline transition data for these variants (Figs. 4B and S1).

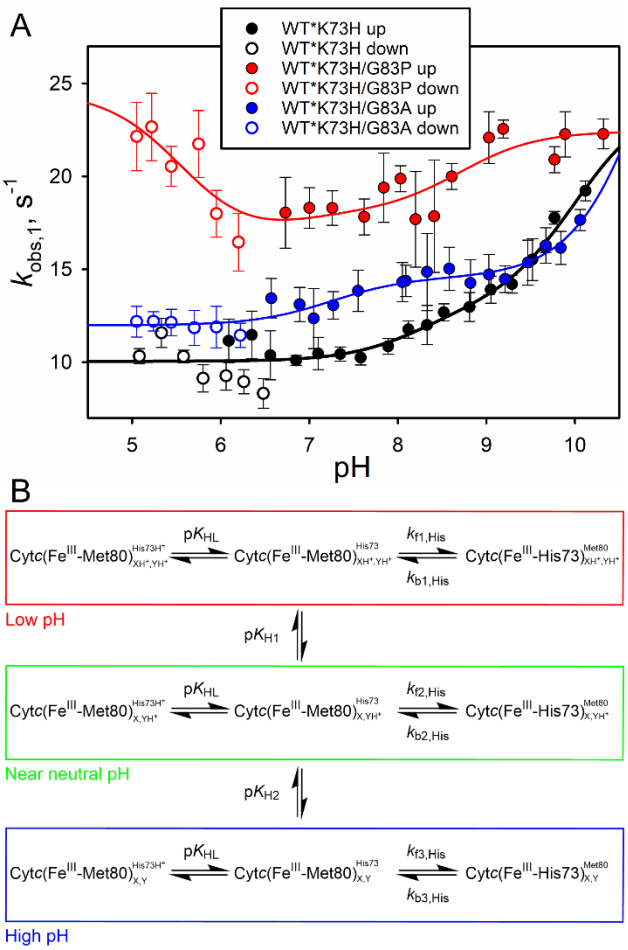

Fig. 5. (A) Plots of $k_{obs,1}$ versus pH for WT*K73H iso-1-Cyt*c* and the G83A and G83P variants of WT*K73H iso-1-Cyt*c*. Data were collected at 25 ºC. The data for WT*/K73H iso-1-Cyt*c* are from McClelland *et al*. [48] and are reproduced here to allow comparison with the G83A and G83P variants of WT*K73H iso-1-Cyt*c*. The solid red curve is a fit of eq. 4 to the data for the WT*K73H/G83P variant and the solid black and blue curves are fits of eq. 5 to the data for WT*K73H iso-1-Cyt*c* the G83A variant of WT*K73H iso-1-Cyt*c*, respectively. (B) Kinetic model used to analyze the data in panel A.

Fig. 5 shows a plot of $k_{obs,1}$ versus pH for the G83A and G83P variants of WT*K73H iso-1-Cyt*c*. One notable difference is that $k_{obs,1}$ is uniformly higher for the WT*K73H/G83P variant than for WT*K73H iso-1-Cyt*c* and the WT*K73H/G83A variant. Also, $k_{obs,1}$ for WT*K73H/G83P iso-1-Cyt*c* decreases from pH 5 to 6 much like for the K73H variant of yeast-expressed iso-1-Cyt*c* (Fig. S4) with tml72 [65]. The pH-dependent behavior of $k_{obs,1}$ for the WT*K73H/G83P iso-1-Cyt*c* variant indicates that it is consistent with the kinetic model we

developed for yeast-expressed K73H iso-1-Cyt*c* [43,65]. In this model (Fig. 5B), the forward rate constant is gated by an ionizable trigger group (pK_{HL}) much like in the standard kinetic model of the alkaline transition [66]. However there are two other ionizable groups that modulate the magnitude of the forward and reverse rate constants one with a pK_a below pK_{HL} (pK_{H1}) and the other with a pK_a higher than pK_{HL} (pK_{H2}). In previous work, we have attributed the pK_{H1} and pK_{H2} [67] to the heme propionates because the observed values of pK_{H1} are typically been 5 and 6 and that of pK_{H2} is near 9 [62,67]. One heme propionate has been reported to have a pK_a < 5 and the other > 9 [16,68,69]. Other studies suggest a role for the heme propionates in triggering the alkaline transition [32], but other ionizable groups including Tyr67, a buried water molecule and His18 have been suggested to be involved in triggering this conformational change [32,61]. This kinetic model leads to eq. 4, where $k_{f1,His}$ and $k_{b1,His}$ are the forward and backward rate

$$(4)\quad k_{obs,1} = \left(\frac{K_{HL}}{K_{HL} + [H^+]}\right)\left(\frac{k_{f1,His}[H^+]^2 + k_{f2,His}K_{H1}[H^+] + k_{f3,His}K_{H1}K_{H2}}{[H^+]^2 + K_{H1}[H^+] + K_{H1}K_{H2}}\right) + \left(\frac{k_{b1,His}[H^+]^2 + k_{b2,His}K_{H1}[H^+] + k_{b3,His}K_{H1}K_{H2}}{[H^+]^2 + K_{H1}[H^+] + K_{H1}K_{H2}}\right)$$

constants for the His73-mediated alkaline transition at pH values below pK_{H1} (because pK_{H1} is less than pK_{HL}, $k_{obs,1}$ is predominately due to $k_{b1,His}$ in this pH regime), $k_{f2,His}$ and $k_{b2,His}$ are the forward and backward rate constants for the His73-mediated alkaline transition at pH values between pK_{H1} and pK_{H2} and $k_{f3,His}$ and $k_{b3,His}$ are the forward and backward rate constants for the His73-mediated alkaline transition at pH values above pK_{H2}. The fit of the data to eq. 4 yields values for pK_{H1}, pK_{HL} and pK_{H2} that are within error of the values observed for yeast-expressed K73H iso-1-Cyt*c* (Table 4).

Table 4

Rate and ionization constants for the His73-mediated alkaline transition of yeast WT* K73H variants of iso-1-Cyt*c* at 25 °C in 10 mM buffer, 0.1 M NaCl.

	Variant			
Parameter	Yeast K73H [a]	WT*K73H/G83P [b]	WT*K73H [c]	WT*K73H/G83A [d]
		Rate Constants, s^{-1}		
$k_{f1,His}$	11.4 ± 0.9	3.7 ± 0.4	-	-
$k_{b1,His}$	23 ± 0.2	25 ± 3	-	-
$k_{f2,His}$	3.5 ± 0.2	2.4 ± 0.2	3 ± 2	2.6 ± 0.3
$k_{b2,His}$	7.0 ± 0.4	15.6 ± 1.5	10.0 ± 0.2	12.0 ± 0.25
$k_{f3,His}$	6.6 ± 0.2	8.2 ± 0.3	12 ± 3	8 ± 19
$k_{b3,His}$	13.2 ± 0.4	14.2 ± 0.5	13 ± 9	29 ± 66
		Ionization Constants		
pK_{H1}	5.6 ± 0.2	5.6 ± 0.4	-	-
pK_{HL}	6.4 ± 0.5	6.7 ± 1.5	8.2 ± 0.6 (6.8 ± 0.1) [e]	7.2 ± 0.2
pK_{H2}	8.7 ± 0.2	8.7 ± 0.6	10.0 ± 0.6 (9.9 ± 0.2) [e]	10.9 ± 1.9

[a] The parameters are from Martinez and Bowler [65].
[b] The ratio k_{f1}/k_{b1} and k_{f2}/k_{b2} were constrained to 0.15 based on the magnitude of pK_C(H73). The ratio k_{f3}/k_{b3} was constrained to 0.58 based on the increase in the amplitude of the His73 kinetic phase from pH 8.03 to 10.32 in pH jump experiments as described in McClelland *et al*. [48].
[c] Parameters are from McClelland *et al*. [48].
[d] The ratio k_{f1}/k_{b1} and k_{f2}/k_{b2} were constrained to 0.08 based on the magnitude of pK_C(H73). The ratio k_{f3}/k_{b3} was constrained to 0.29 based on the increase in the amplitude of the His73 kinetic phase from pH 8.03 to 10.32 in pH jump experiments as described in McClelland *et al*. [48].
[e] Parameters from amplitude data [48].

The $k_{obs,1}$ versus pH data for WT*K73H/G83A iso-1-Cyt*c* is more similar to the data observed for the WT*K73H variant. The magnitude of $k_{obs,1}$ is more similar across the pH range and there is no clear decrease in $k_{obs,1}$ between pH 5 and 6 as observed for yeast-expressed K73H iso-1-Cyt*c* and the WT* K73H/G83P variant. Thus, a kinetic model without pK_{H1} (see Fig. 5B) was applied to the data. This model yields eq. 5. A fit of eq. 5 to the data for WT*K73H/G83A

$$(5)\quad k_{\mathrm{obs,1}} = \left(\frac{K_{\mathrm{HL}}}{K_{\mathrm{HL}} + [\mathrm{H^+}]}\right)\left(\frac{k_{\mathrm{f2,His}}[\mathrm{H^+}] + k_{\mathrm{f3,His}}K_{\mathrm{H2}}}{[\mathrm{H^+}] + K_{\mathrm{H2}}}\right) + \left(\frac{k_{\mathrm{b2,His}}[\mathrm{H^+}] + k_{\mathrm{b3,His}}K_{\mathrm{H2}}}{[\mathrm{H^+}] + K_{\mathrm{H2}}}\right)$$

iso-1-Cyt*c* yields similar values for pK_{HL} and pK_{H2} as reported previously for the WT*K73H iso-1-Cyt*c* [48]. For all variants, pK_{HL} is near 7 consistent with ionization of His73 being the triggering ionization for the His73-mediated alkaline transition. The magnitude of pK_{H2} for WT*K73H iso-1-Cyt*c* and the WT*K73H/G83A variant appears to be higher than for yeast-expressed K73H iso-1-Cyt*c* and the WT*K73H/G83P variant. Although, pK_{H2} and the associated $k_{\mathrm{f3,His}}$ and $k_{\mathrm{b3,His}}$ rate constants are poorly determined for the WT*K73H/G83A because $k_{\mathrm{obs,1}}$ does not level off at the highest pH values in our dataset.

The pH dependence of $k_{\mathrm{obs,3}}$ and the amplitudes of this kinetic phase for WT*K73H/G83P and WT*K73H/G83A are shown in Fig. S5. The equations for the standard model for the kinetics of the alkaline conformational transition [66] were fit to the data yielding the parameters reported in Table 5. The values of pK_{H} in Table 5 derived from rate constant and amplitude data are in good agreement and the magnitudes of pK_{C}(K79) derived from the kinetic data are similar to those obtained from equilibrium titrations (Table 3).

Table 5
Kinetic parameters for the Lys79-mediated transition of WT*K73H iso-1-Cyt*c* and variants at 25 °C.

Variant	$k_{\mathrm{f,Lys79}}$, $\mathrm{s^{-1}}$	$k_{\mathrm{b,Lys79}}$, $\mathrm{s^{-1}}$	pK_{C}(K79) [b]	pK_{H}
WT*K73H [a]	0.50 ± 0.04	0.015 ± 0.003	-1.5 ± 0.2	9.94 ± 0.07 (9.87 ± 0.07) [c]
WT*K73H/G83A	0.64 ± 0.02	0.0120 ± 0.0005	-1.73 ± 0.04	10.09 ± 0.02 (10.07 ± 0.08) [c]
WT*K73H/G83P	0.45 ± 0.01	0.010 ± 0.001	-1.64 ± 0.12	9.91 ± 0.03 (9.84 ± 0.12) [b]

[a] Data from McClelland *et al*. [48]. Fitted parameters were not reported in this publication.

[b] Calculated as pK_{C}(K79) = $-\log(k_{\mathrm{f,Lys79}}/k_{\mathrm{b,Lys79}})$. Error is from standard propagation of the errors in the rate constants.

[c] From amplitude data.

*3.3. Gated electron transfer data for WT*K73H/G83P iso-1-Cytc*

To further characterize the kinetics of the His73-mediated alkaline transition of WT*K73H/G83P iso-1-Cyt*c*, we used gated electron transfer (ET) methods [49,50,67,70,71]. Gated ET experiments provide an excellent method to directly measure the rate constant for the return from the His73-heme alkaline state to the native state using hexammineruthenium(II), a_6Ru^{2+}. Because the redox potential for the heme of Cyt*c* decreases by about 250 mV when Met80 is replaced by His73 as the heme ligand, the His73-heme alkaline conformer cannot be reduced directly by a_6Ru^{2+}. At sufficiently high concentrations of a_6Ru^{2+}, the rate of reduction of the native conformer is fast compared to the rate of the conformational change from the His73-heme alkaline conformer to the native conformer. Thus, reduction of the His73-heme alkaline conformer is limited by the conformational change to the native state (Fig. 6B).

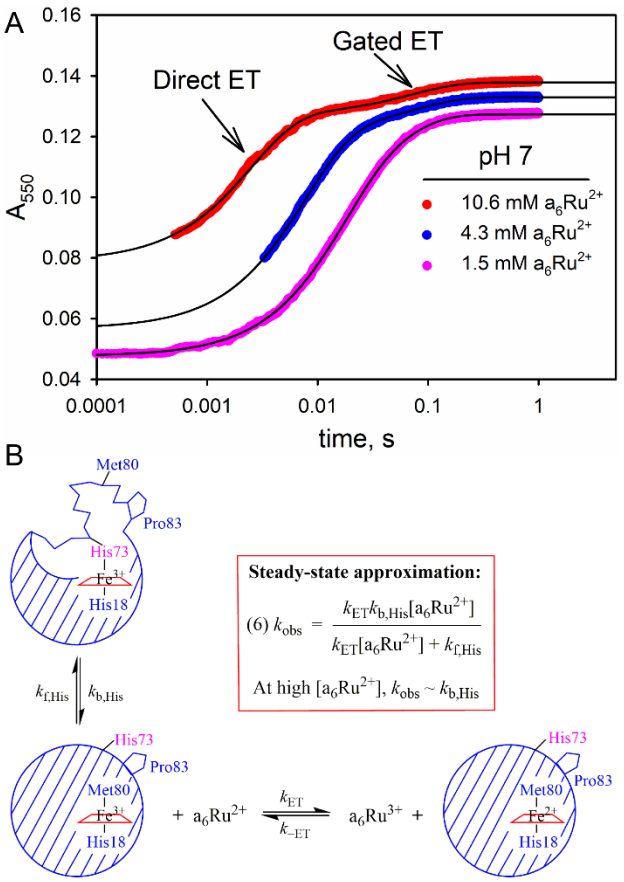

Fig. 6. Gated ET on WT*K73H/G83P iso-1-Cyt*c*. (A) Reduction of WT*K73H/G83P iso-1-Cyt*c* as a function of a_6Ru^{2+} concentration monitored at 550 nm and 25 ºC. (B) Kinetic scheme for gated ET.

At pH 7, WT*K73H/G83P iso-1-Cyt*c* is primarily a mixture of the native state and the His73-heme alkaline conformer. Thus when it is reacted with a_6Ru^{2+}, direct ET to the native state is expected as well as gated ET from the His73-heme alkaline conformer. The latter will be limited by $k_{b,His}$. Fig. 6A shows reduction of the WT*K73H/G83P iso-1-Cyt*c* as a function of a_6Ru^{2+} concentration at pH 7. As expected two kinetic phases are observed. The fastest phase (k_{gET1}) depends on a_6Ru^{2+} concentration (Table S6) and thus can be assigned to direct ET to the native state in a bimolecular reaction. A plot of k_{gET1} versus a_6Ru^{2+} concentration (Fig. S6A) yields a value of 38 ± 3 mM^{-1} s^{-1} for k_{ET}. This value compares well with k_{ET} at pH 7 of 42.4 ± 0.5

mM^{-1} s^{-1} observed previously for WT*K73H [48]. A plot of the slow phase of reduction (k_{gET2}) versus a_6Ru^{2+} concentration shows that k_{gET2} is essentially invariant with a_6Ru^{2+} concentration (Fig. S6B). Eq. 6 in Fig. 6 can be fit to the data, yielding $k_{b,His} = 15.4 \pm 0.6$ s^{-1}. A value of 0.9 ± 2.4 is obtained for $k_{f,His}$. The error in $k_{f,His}$ is large because the data poorly constrain this parameter. A better way to obtain $k_{f,His}$ is to use $k_{obs,1}$ (equals $k_{f,His} + k_{b,His}$) from pH jump data near pH 7. The average and standard deviation of the $k_{obs,1}$ from pH jump data between pH 6.7 and 7.3 is 18.2 ± 0.2. Therefore, we obtain $k_{f,His} = 2.8 \pm 0.6$ s^{-1}.These values compare well to the value we would expect near pH 7 based on the fit of eq. 5 to our pH jump stopped-flow data (Fig. 5 and Table 4) which yielded $k_{f,His2} = 2.4 \pm 0.2$ s^{-1} and $k_{b,His2} = 15.6 \pm 1.5$ s^{-1}. Using these values for $k_{f,His2}$ and $k_{b,His2}$, to calculate pK_C(H73) near pH 7, yields 0.74 ± 0.09, which agrees well with pK_C(H73) obtained from thermodynamic data (Table 3).

When the data collection is extended out to 200 s or more a third phase yields a rate constant, k_{gET3}, of about 0.029 s^{-1} that is also invariant with a_6Ru^{2+} concentration. This rate is similar to $k_{b,Lys79} = 0.010 \pm 0.001$ s^{-1} extracted from the slow phase of the pH jump stopped-flow experiments. Thus, it is likely due to gated ET from a small population of the Lys79-heme alkaline state at pH 7.

3.4. Peroxidase activity measurements on variants of iso-1-Cytc containing His73

Because histidine ligation is thought to occur when Cyt*c* binds to cardiolipin-containing membranes [72-74], it is of interest to measure the peroxidase activity of WT*K73H iso-1-Cyt*c* and variants of this protein containing the G83A and G83P mutations since these variants change the favorability of binding His73 to the heme. Thus, the effect of histidine ligation on the peroxidase activity of Cyt*c* that promotes apoptosis in its early stages can be ascertained.

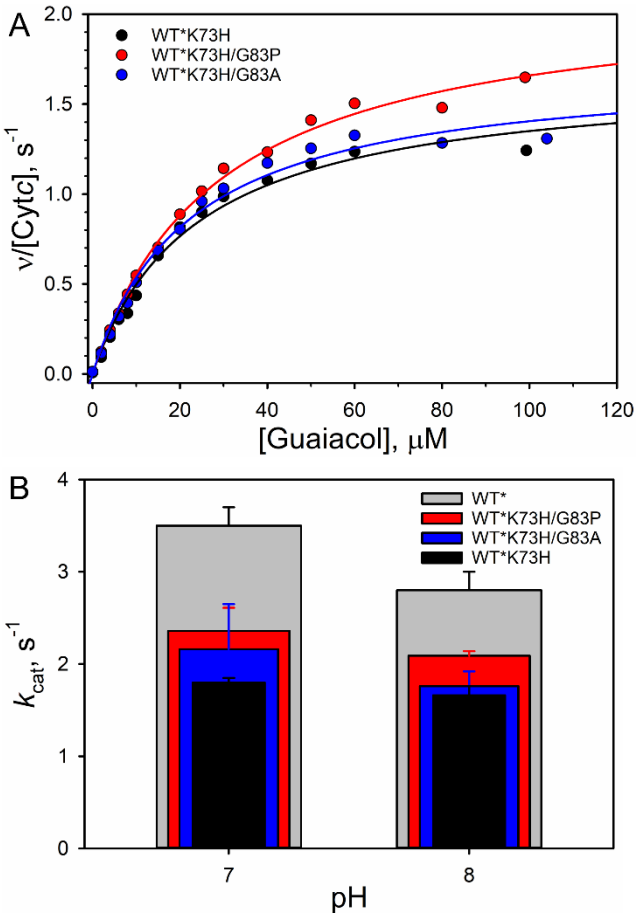

Fig. 7. Peroxidase activity of iso-1-Cyt*c* variants. (A) Plots of initial rate divided by protein concentration, v/[Cyt*c*], versus guaiacol concentration. Solid lines are fits of the Michaelis-Menten equation to the data. (B) Values of k_{cat} at pH 7 and pH 8 for WT* and His73 containing variants of iso-1-Cyt*c*. All data were obtained at 25 °C.

The peroxidase activity of all three variants using guaiacol as substrate can be fit well by the Michaelis-Menten equation (Fig. 7A). Measurements were carried out at pH 7 where His73 is expected to be the primary alkaline state ligand and at pH 8, where Lys79 should begin to contribute to heme ligation (see Figs. 4 and S1). Relative to the WT* iso-1-Cyt*c*, the magnitude of k_{cat} for WT*K73H iso-1-Cyt*c* decreases significantly at both pH 7 ($p = 0.00016$) and 8 ($p = 0.0047$, Fig. 7B and Table 6). The k_{cat} values of the G83P and G83A variants of WT*K73H are also decreased compared to WT* (pH 7: p(G83P) = 0.0014, p(G83A) = 0.013; pH 8: p(G83P) =

0.010, p(G83A) = 0.0013), although the G83P mutation partially restored the peroxidase activity, with a k_{cat} significantly higher than WT*K73H at pH 7 (p = 0.014) and 8 (p = 0.013). However, for the WT*K73H/G83A variant the changes in k_{cat} are within error of k_{cat} for WT*K73H iso-1-Cyt*c* (p-values > .05). The Michaelis constants, K_m, obtained are consistent with previous work with the WT* variant. Thus, the trends in k_{cat}/K_m are similar to those for k_{cat} (Table 6).

Table 6
Michaelis-Menten parameters for peroxidase activity of iso-1-Cyt*c* variants at 25 ºC.

Variant	pH 7			pH 8		
	k_{cat}, s^{-1}	K_m, μM^{-1}	k_{cat}/K_m, $M\ s^{-1}$	k_{cat}, s^{-1}	K_m, μM^{-1}	k_{cat}/K_m, $M\ s^{-1}$
WT* [a]	3.5 ± 0.2	16 ± 1	2.2 ± 0.1 x10^5	2.8 ± 0.2	25 ± 1	1.12 ± 0.06 x10^5
WT*K73H	1.80 ± 0.05	17 ± 3	1.0 ± 0.2 x10^5	1.7 ± 0.1	25 ± 2	6.6 ± 0.4 x10^4
WT*K73H/G83P	2.4 ± 0.3	16 ± 4	1.4 ± 0.4 x10^5	2.09 ± 0.05	29 ± 1	7.2 ± 0.2 x10^4
WT*K73H/G83A	2.2 ± 0.5	13 ± 1	1.7 ± 0.4 x10^5	1.8 ± 0.2	22 ± 4	7.8 ± 0.7 x10^4

[a] Parameters are McClelland *et al* [75].

4. Discussion

4.1. Effect of Pro83 on the thermodynamics and kinetics of the His73 alkaline state

One goal of this study was to evaluate the effect of substitution of a proline into position 83 of Ω-loop on the dynamics of this loop, which is critical for both the ET function of Cyt*c* and its peroxidase activity in the early stages of apoptosis. There is some evidence that proline-rich loops stiffen the protein backbone near heme cofactors [22,24]. However, other research suggest that prolines can enhance fluxional behavior near heme cofactors [25,26].

To address the effect of the G83P mutation on the energy landscape of Ω-loop D, it is useful to establish the impact of the mutation on the native versus the His73-mediated alkaline conformer. In previous work, we have observed that GdnHCl unfolding of iso-1-Cyt*c* variants containing a K73H mutation measures unfolding from the His73 alkaline state when monitored by CD spectroscopy [60]. These variants typically have a GdnHCl *m*-value near 3.5 kcal $mol^{-1}M^{-1}$ [35,43,60], whereas WT* iso-1-Cyt*c* has an *m*-value near 4.4 kcal $mol^{-1}M^{-1}$ [48]. In Table 1, all the variants containing the K73H mutation have *m*-values of 3.5 kcal $mol^{-1}M^{-1}$ or less. All variants lacking the K73H mutation have *m*-values ranging from 4.1 to 4.4 kcal $mol^{-1}M^{-1}$. This observation indicates that GdnHCl unfolding on the variants containing the K73H mutation is measuring the stability of the His73 alkaline conformer. The data in Fig. 1 and Table 1 show that WT*K73H and the G83A and G83P variants of this protein have identical stabilities. Therefore, in building an energy landscape for the dynamics of the His73-mediated alkaline transition, we will assume that the G83P mutation does not affect the stability of the His73 alkaline conformer (see Fig. 8). The difference in the pK_C(H73) parameters for WT*K73H compared to WT*K73H/G83P indicates that the native conformer of the WT* K73H/G83P is ~0.2 kcal/mol more stable than that of WT*K73H iso-1-Cyt*c*.

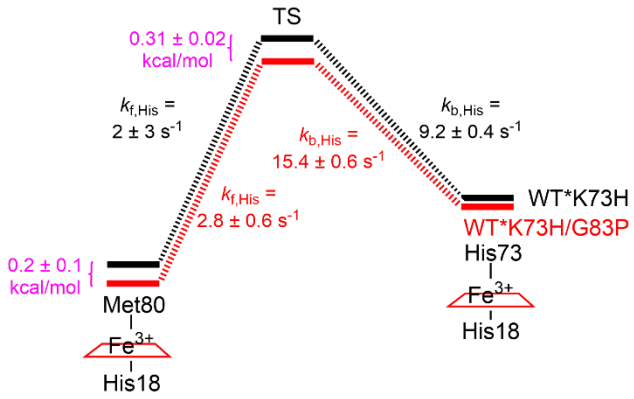

Fig. 8. Energy level diagram showing the effect of the G83P mutation on the thermodynamics and kinetics of the His73-mediated alkaline transition. The $k_{f,His}$ and $k_{b,His}$ rate constants for the WT*K73H variant at pH 7 are from McClelland *et al* [48].

Gated ET measurements allowed us to determine $k_{b,His}$ with good precision at pH 7 for both WT*K73H [48] and WT*K73H/G83P. Using transition state (TS) theory and the magnitude of this rate constant for each of these variants, we can obtain a precise value for the stabilization of the free energy of the TS, caused by the G83P mutation, for the His73-mediated alkaline transition with respect to the His73 alkaline conformer. We find this stabilization to be 0.31 ± 0.02 kcal/mol. Although, $k_{f,His}$ is not well-determined for the WT*K73H variant [48], the stabilization of the TS and the native state by the G83P mutation are consistent with $k_{f,His}$ being essentially the same for WT*K73H iso-1-Cyt*c* and WT*K73H/G83P variant. Thus, in terms of the dynamics of opening up the native state conformer, the G83P mutation appears to be neutral (i.e. it does not stiffen the backbone of the native state). The faster dynamics observed for the WT*K73H/G83P variant in pH jump stopped-flow experiments (Fig. 5) result entirely from a stabilization of the TS with respect to the His73-heme conformer.

4.2 Effect of His73 ligation on peroxidase activity

A number of studies have shown that when Cyt*c* binds to CL-containing membranes, it forms bis-His ligated states [72-74]. Because oxygenation of CL by Cyt*c* is an important early signal in apoptosis, the effect of the bis-His ligated state of Cyt*c* bound to CL on the peroxidase activity of Cyt*c* is important to evaluate. From the data in Table 6 and Fig. 7B, it is evident that bis-His ligation inhibits peroxidase activity. Our data suggest that transiently populated states for WT* iso-1-Cyt*c* near neutral pH which lack Met80 ligation are readily quenched by an available histidine ligand. At higher pH, the Lys-mediated alkaline states also block the peroxidase activity of Cyt*c* [52,76]. Thus, it appears that replacement of Met80 by a strong field ligand is a general inhibitor of the peroxidase activity of Cyt*c*.

It has been shown that a bis-His ligated state of urea-denatured yeast iso-1-Cyt*c* can lead to pseudo-peroxidase activity on electrodes coated with anionic self-assembled monolayers (SAM) [77]. In this case the mechanism of pseudo-peroxidase activity involves an initial reduction of iso-1-Cyt*c*, which weakens the iron bond to histidine. In our case, peroxidase activity most likely involves peroxide binding directly to the Fe(III)-heme followed by formation of compound I (Fe(IV)-heme) [78]. Thus, weakening of histidine ligation by reduction is unlikely involved for our peroxidase activity measurements. Recent data on CL vesicles show that the local pH at the surface of the vesicle is near 4 when the bulk pH is near pH 6.8 [79] (similar to the pH in the cristae of mitochondria [80]). This pH would be sufficient to convert the bis(His) ligation observed in urea or GdnHCl-denatured Cyt*c* to His-Fe(III)-OH_2 ligation [60,81]. However, spectroscopic data provide convincing evidence that bis(His) ligation occurs when Cyt*c* is bound to CL vesicles near neutral pH [72-74] despite the low local pH. This observation suggests that Cyt*c* is not fully unfolded when bound to CL vesicles and is thus more resistant to cleavage of

the His-heme bond that replaces Met80 heme ligation. However, we note that the histidine ligand (His 26 or 33) that replaces Met80 when WT horse Cyt*c* binds to a CL-containing vesicle [72-74] comes from a different Ω-loop than the one probed in these studies.

Our data can also address the question of whether peroxidase activity depends only on the rate of loss of the Met80-ligated state or if it is also controlled by the equilibrium accessibility of peroxidase-competent states. For WT*K73H iso-1-Cyt*c* and the WT*K73H/G83P variant, the rate constant for loss of Met80-ligation ($k_{f,His}$) is essentially the same as noted in section 4.1. However, the equilibrium population of the His73-heme conformer is lower for the WT*K73H/G83P variant than for WT*K73H iso-1-Cyt*c* (Table 3). In Fig. 7B and Table 6, the peroxidase activity of the WT*K73H/G83P is higher than that of WT*K73H at both pH 7 and 8. These observations suggest that the equilibrium population of the His73-ligated state is the predominant factor in controlling the peroxidase activity of iso-1-Cyt*c*. The His73-ligated state blocks peroxidase activity and the loss of activity appears to correlate with its equilibrium population. However, we cannot rule out the possibility that the peroxidase activity could be kinetically controlled on a lipid bilayer containing CL.

5. Conclusion

Using K73H variants of iso-1-Cyt*c* with and without a proline substitution at position 83, we have shown that proline at this position enhances the dynamics of Ω-loop D. However, the enhanced dynamics do not affect the rate of opening of Ω-loop D, but instead primarily result from an increase in the rate of return to the Met80-ligated state. Our results also show that bis-His ligation inhibits the peroxidase activity of Cyt*c*, much like His/Lys ligation. Thus, the bis-

His ligated state observed upon binding to CL-containing membranes is likely a negative effector of the peroxidase activity of Cyt*c* that is essential in the early stages of apoptosis.

Abbreviations

CD	circular dichroism
Cyt*c*	cytochrome *c*
ET	electron transfer
Gated ET	conformationally-gated electron transfer
$\Delta G_u°'(H_2O)$	free energy of unfolding in the absence of denaturant
GdnHCl	guanidine hydrochloride
iso-1-Cyt*c*	yeast iso-1-cytochrome *c*
m	slope of a plot of free energy of unfolding versus denaturant concentration
tml72	trimethyllysine 72
WT*	variant of yeast iso-1-Cyt*c* with K72A and C102S substitutions

Declaration of Competing Interest

The authors declare that they have no known competing financial interests or personal relationships that could have appeared to influence the work reported in this paper.

Acknowledgements

This research was supported a grants from the NSF [CHE-0910166 and CHE-1904895 (B.E.B.)].

Appendix A. Supplementary data

Supplementary data to this article can be found online at

References

[1] T.E. Creighton Proteins: Structure and Molecular Properties, W. H. Freeman and Co., New York, 1984.

[2] G.D. Rose, L.M. Gierasch, J.A. Smith. Turns in peptides and proteins, Adv. Protein Chem. 37 (1985) 1-109.

[3] R. Aurora, G.D. Rose. Helix capping, Protein Sci. 7 (1998) 21-38.

[4] Y. Suzuki. The proline rule: a strategy for protein thermal stabilization, Proc. Japan Acad., Ser. B Phys. Biol. Sci. 75 (1999) 133-137.

[5] Y. Suzuki, in: A. Svendsen (Ed.), Enzyme Functionality: Design, Engineering, and Screening, Marcel Dekker, Inc., New York, 2004, pp. 293 - 323.

[6] S.R. Trevino, S. Schaefer, J.M. Scholtz, C.N. Pace. Increasing protein conformational stability by optimizing beta-turn sequence, J. Mol. Biol. 373 (2007) 211-218.

[7] B.W. Matthews, H. Nicholson, W.J. Becktel. Enhanced protein thermostability from site-directed mutations that decrease the entropy of unfolding, Proc. Natl. Acad. Sci. U.S.A. 84 (1987) 6663-6667.

[8] C.R. Cantor, P.R. Schimmel Biophysical Chemistry, Part III: The Behavior of Biological Macromolecules, W. H. Freeman and Co., San Francisco, 1980.

[9] F. Krieger, A. Möglich, T. Kiefhaber. Effect of proline and glycine residues on dynamics and barriers of loop formation in polypeptide chains, J. Am. Chem. Soc. 127 (2005) 3346-3352.

[10] K. Henzler-Wildman, D. Kern. Dynamic personalities of proteins, Nature 450 (2007) 964-972.

[11] P.O. Byrne, J.S. McLellan. Principles and practical applications of structure-based vaccine design, Curr. Opin. Immunol. 77 (2022) 102209.

[12] D. Wrapp, N. Wang, K.S. Corbett, J.A. Goldsmith, C.-L. Hsieh, O. Abiona, B.S. Graham, J.S. McLellan. Cryo-EM structure of the 2019-nCoV spike in the prefusion conformation, Science 367 (2020) 1260-1263.

[13] J. Pallesen, N. Wang, K.S. Corbett, D. Wrapp, R. Kirchdoerfer, N., H. Turner, L., C. Cottrell, A., M. Becker, M., L. Wang, W. Shi, W.-P. Kong, E. Andres, L., A. Kettenbach, N., M. Denison, R., J. Chappell, D., B. Graham, S., A. Ward, B., J. McLellan, S. Immunogenicity and structures of a rationally designed prefusion MERS-CoV spike antigen, Proc. Natl. Acad. Sci. U.S.A. 114 (2017) E7348-E7357.

[14] M.T. Rothfuss, D.C. Becht, B. Zeng, L.J. McClelland, C. Yates-Hansen, B.E. Bowler. High-accuracy prediction of stabilizing surface mutations to the three-helix bundle, UBA(1), with EmCAST, J. Am. Chem. Soc. 145 (2023) 22979-22992.

[15] V.E. Kagan, V.A. Tyurin, J. Jiang, Y.Y. Tyurina, V.B. Ritov, A.A. Amoscato, A.N. Osipov, N.A. Belikova, A.A. Kapralov, V. Kini, I.I. Vlasova, Q. Zhao, M. Zou, P. Di, D.A. Svistunenko, I.V. Kurnikov, G.G. Borisenko. Cytochrome *c* acts as a cardiolipin oxygenase required for release of proapoptotic factors, Nat. Chem. Biol. 1 (2005) 223-232.

[16] G.R. Moore, G.W. Pettigrew Cytochromes *c*: Evolutionary, Structural and Physicochemical Aspects, Springer-Verlag, New York, 1990.

[17] L. Banci, I. Bertini, A. Rosato, G. Varani. Mitochondrial cytochromes *c*: a comparative analysis, J. Biol. Inorg. Chem. 4 (1999) 824-837.

[18] L. Banci, I. Bertini, S. Ciurli, A. Dikiy, J. Dittmer, A. Rosato, G. Sciara, A.R. Thompsett. NMR solution structure, backbone mobility, and homology modeling of *c*-type cytochromes *c* from gram-positive bacteria, ChemBioChem 3 (2002) 299-310.

[19] I. Bartalesi, I. Bertini, K. Ghosh, A. Rosato, P. Turano. The unfolding of oxidized *c*-type cytochromes: the instructive case of *Bacillus pasteurii*, J. Mol. Biol. 321 (2002) 693-701.

[20] I. Bartalesi, I. Bertini, A. Rosato. Structure and dynamics of reduced *Bacillus pasteurii* cytochrome *c*: oxidation state dependent properties and implications for electron transfer processes, Biochemistry 42 (2003) 739-745.

[21] I. Bartalesi, I. Bertini, G. Di Rocco, M. Vanarotti, P.R. Vasos, M.S. Viezzoli. Protein stability and mutations in the axial methionine loop of a minimal cytochrome *c*, J. Biol. Inorg. Chem. 9 (2004) 600-608.

[22] B.S. Russell, L. Zhong, M.G. Bigotti, F. Cutruzzola, K.L. Bren. Backbone dynamics and hydrogen exchange of *Pseudomonas aeruginosa* ferricytochrome c_{551}, J. Biol. Inorg. Chem. 8 (2003) 156-166.

[23] M. Cai, E.G. Bradford, R. Timkovich. Investigation of the solution conformation of cytochrome *c*-551 from Pseudomonas stutzeri, Biochemistry 31 (1992) 8603-8612.

[24] L.V. Michel, K.L. Bren. Submolecular unfolding units of *Pseudomonas aeruginosa* cytochrome c_{551}, J. Biol. Inorg. Chem. 13 (2008) 837-845.

[25] K.L. Bren, J.A. Kellogg, R. Kaur, X. Wen. Folding, conformational changes, and dynamics of cytochromes *c* probed by NMR spectroscopy, Inorg. Chem. 43 (2004) 7934-7944.

[26] L. Zhong, X. Wen, T.M. Rabinowitz, B.S. Russell, E.F. Karan, K.L. Bren. Heme axial methionine fluxionality in Hydrogenobacter thermophilus cytochrome c_{552}, Proc. Natl. Acad. Sci. U.S.A. 101 (2004) 8637-8642.

[27] A.M. Berghuis, G.D. Brayer. Oxidation state-dependent conformational changes in cytochrome *c*, J. Mol. Biol. 223 (1992) 959-976.

[28] W.L. DeLano. The PyMOL molecular graphics system, Version 1, DeLano Scientific, LLC, San Carlos, CA, USA (2006)

[29] G.E. Crooks, G. Hon, J.-M. Chandonia, S.E. Brenner. WebLogo: a sequence logo generator, Genome Res. 14 (2004) 1188-1190.

[30] S. Bandi, B.E. Bowler. Effect of an Ala81His mutation on the Met80 loop dynamics of iso-1-cytochrome *c*, Biochemistry 54 (2015) 1729−1742.

[31] H. Lei, S.M. Nold, L. Jung Motta, B.E. Bowler. Effect of V83G and I81A substitutions to human cytochrome *c* on acid unfolding and peroxidase activity below neutral pH, Biochemistry 58 (2019) 2921−2933.

[32] O.M. Deacon, D.A. Svistunenko, G.R. Moore, M.T. Wilson, J.A.R. Worrall. Naturally occurring disease-related mutations in the 40−57 Ω-loop of human cytochrome *c* control triggering of the alkaline isomerization, Biochemistry 57 (2018) 4276−4288.

[33] H. Lei, B.E. Bowler. Humanlike substitutions to Ω-loop D of yeast iso-1-cytochrome *c* only modestly affect dynamics and peroxidase activity, J. Inorg. Biochem. 183 (2018) 146-156.

[34] L. Hoang, H. Maity, M.M. Krishna, Y. Lin, S.W. Englander. Folding units govern the cytochrome *c* alkaline transition, J. Mol. Biol. 331 (2003) 37-43.

[35] R. Kristinsson, B.E. Bowler. Communication of stabilizing energy between substructures of a protein, Biochemistry 44 (2005) 2349-2359.

[36] M.G. Duncan, M.D. Williams, B.E. Bowler. Compressing the free energy range of substructure stabilities in iso-1-cytochrome *c*, Protein Sci. 18 (2009) 1155-1164.

[37] J.N. Rumbley, L. Hoang, S.W. Englander. Recombinant equine cytochrome *c* in *Escherichia coli*: high-level expression, characterization, and folding and assembly mutants, Biochemistry 41 (2002) 13894-13901.

[38] F.I. Rosell, A.G. Mauk. Spectroscopic properties of a mitochondrial cytochrome *c* with a single thioether bond to the heme prosthetic group, Biochemistry 41 (2002) 7811-7818.

[39] W.B. Pollock, F.I. Rosell, M.B. Twitchett, M.E. Dumont, A.G. Mauk. Bacterial expression of a mitochondrial cytochrome *c*. Trimethylation of Lys72 in yeast iso-1-cytochrome *c* and the alkaline conformational transition, Biochemistry 37 (1998) 6124-6131.

[40] R.L. Cutler, G.J. Pielak, A.G. Mauk, M. Smith. Replacement of cysteine-107 of *Saccharomyces cerevisiae* iso-1-cytochrome *c* with threonine: improved stability of the mutant protein, Protein Eng. Des. Sel. 1 (1987) 95-99.

[41] M.M. Cherney, C. Junior, B.E. Bowler. Mutation of trimethyllysine-72 to alanine enhances His79-heme mediated dynamics of iso-1-cytochrome *c*, Biochemistry 52 (2013) 837-846.

[42] S. Bandi, S. Baddam, B.E. Bowler. Alkaline conformational transition and gated electron transfer with a Lys 79 -> His variant of iso-1-cytochrome *c*, Biochemistry 46 (2007) 10643-10654.

[43] S. Baddam, B.E. Bowler. Thermodynamics and kinetics of formation of the alkaline state of a Lys 79->Ala/Lys 73->His variant of iso-1-cytochrome *c*, Biochemistry 44 (2005) 14956-14968.

[44] M.M. Santoro, D.W. Bolen. A test of the linear extrapolation of unfolding free energy changes over an extended denaturant concentration range, Biochemistry 31 (1992) 4901-4907.

[45] Y. Hagihara, Y. Tan, Y. Goto. Comparison of the conformational stability of the molten globule and native states of horse cytochrome *c*, J. Mol. Biol. 237 (1994) 336-348.

[46] S. Godbole, B. Hammack, B.E. Bowler. Measuring denatured state energetics: deviations from random coil behavior and implications for the folding of iso-1-cytochrome *c*, J. Mol. Biol. 296 (2000) 217-228.

[47] C.J. Nelson, B.E. Bowler. pH dependence of formation of a partially unfolded state of a Lys 73 -> His variant of iso-1-cytochrome *c*: implications for the alkaline conformational transition of cytochrome *c*, Biochemistry 39 (2000) 13584-13594.

[48] L.J. McClelland, S.M. Seagraves, M.K.A. Khan, M.M. Cherney, S. Bandi, J.E. Culbertson, B.E. Bowler. The response of Ω-loop D dynamics to truncation of trimethyllysine 72 of yeast iso-1-cytochrome *c* depends on the nature of loop deformation, J. Biol. Inorg. Chem. 20 (2015) 805-819.

[49] S. Bandi, B.E. Bowler. A cytochrome *c* electron transfer switch modulated by heme ligation and isomerization of a peptidyl-prolyl bond, Biopolymers 100 (2013) 114-124.

[50] S. Baddam, B.E. Bowler. Conformationally gated electron transfer in iso-1-cytochrome *c*: engineering the rate of a conformational switch, J. Am. Chem. Soc. 127 (2005) 9702-9703.

[51] R.E.M. Diederix, M. Ubbink, G.W. Canters. Peroxidase activity as a tool for studying the folding of *c*-type cytochromes, Biochemistry 41 (2002) 13067-13077.

[52] R.E.M. Diederix, M. Ubbink, G.W. Canters. The peroxidase activity of cytochrome *c*-550 from *Paracoccus versutus*, Eur. J. Biochem. 268 (2001) 4207-4216.

[53] R. Radi, L. Thomson, H. Rubbo, E. Prodanov. Cytochrome *c*-catalyzed oxidation of organic molecules by hydrogen peroxide, Arch. Biochem. Biophys. 288 (1991) 112-117.

[54] S. Samsri, S. Pornsuwan. Influence of cysteine-directed mutations at the Ω-loops on peroxidase activity of human cytochrome c, Arch. Biochem. Biophys. 709 (2021) 108980.

[55] O. Goldschmid. The effect of alkali and strong acid on the ultraviolet absorption spectrum of lignin and related compounds, J. Am. Chem. Soc. 75 (1953) 3780-3783.

[56] R.W. Noble, Q.H. Gibson. The reaction of ferrous horseradish peroxidase with hydrogen peroxide, J. Biol. Chem. 245 (1970) 2409-2413.

[57] D.P. Nelson, L.A. Kiesow. Enthalpy of decomposition of hydrogen peroxide by catalase at 25 °C (with molar extinction coefficients of H_2O_2 solutions in the UV), Anal. Biochem. 49 (1972) 474-478.

[58] D.R. Doerge, R.L. Divi, M.I. Churchwell. Identification of the colored guaiacol oxidation product produced by peroxidases, Anal. Biochem. 250 (1997) 10-17.

[59] J.A. Schellman. Solvent denaturation, Biopolymers 17 (1978) 1305-1322.

[60] S. Godbole, A. Dong, K. Garbin, B.E. Bowler. A lysine 73->histidine variant of yeast iso-1-cytochrome *c*: evidence for a native-like intermediate in the unfolding pathway and implications for *m* value effects, Biochemistry 36 (1997) 119-126.

[61] M.T. Wilson, C. Greenwood, in: R.A. Scott, A.G. Mauk (Eds.), Cytochrome *c*: A Multidisciplinary Approach, University Science Books, Sausalito, CA, 1996, pp. 611-634.

[62] M.M. Cherney, B.E. Bowler. Protein dynamics and function: making new strides with an old warhorse, the alkaline conformational transition of cytochrome *c*, Coord. Chem. Rev. 255 (2011) 664-677.

[63] F.I. Rosell, J.C. Ferrer, A.G. Mauk. Proton-linked protein conformational switching: definition of the alkaline conformational transition of yeast iso-1-ferricytochrome *c*, J. Am. Chem. Soc. 120 (1998) 11234-11245.

[64] M.N. Robinson, A.P. Boswell, Z.-X. Huang, C.G.S. Eley, G.R. Moore. The conformation of eukaryotic cytochrome *c* around residues 39, 57, 59 and 74, Biochem. J. 213 (1983) 687-700.

[65] R.E. Martinez, B.E. Bowler. Proton-mediated dynamics of the alkaline conformational transition of yeast iso-1-cytochrome *c*, J. Am. Chem. Soc. 126 (2004) 6751-6758.

[66] L.A. Davis, A. Schejter, G.P. Hess. Alkaline isomerization of oxidized cytochrome *c*. Equilibrium and kinetic measurements, J. Biol. Chem. 249 (1974) 2624-2632.

[67] S. Bandi, B.E. Bowler. Probing the dynamics of a His73-heme alkaline conformer in a destabilized variant of yeast iso-1-cytochrome *c* with conformationally gated electron transfer methods, Biochemistry 50 (2011) 10027–10040.

[68] R.T. Hartshorn, G.R. Moore. A denaturation-induced proton-uptake study of horse ferricytochrome *c*, Biochem. J. 258 (1989) 595-598.

[69] G.R. Moore. Control of redox properties of cytochrome *c* by special electrostatic interactions, FEBS Lett. 161 (1983) 171-175.

[70] S. Bandi, B.E. Bowler. Probing the bottom of a folding funnel using conformationally gated electron transfer reactions, J. Am. Chem. Soc. 130 (2008) 7540-7541.

[71] S. Baddam, B.E. Bowler. Tuning the rate and pH accessibility of a conformational electron transfer gate, Inorg. Chem. 45 (2006) 6338-6346.

[72] B. Milorey, D. Malyshka, R. Schweitzer-Stenner. pH dependence of ferricytochrome c conformational transitions during binding to cardiolipin membranes: evidence for histidine as the distal ligand at neutral pH, J. Phys. Chem. Lett. 8 (2017) 1993−1998.

[73] L. Milazzo, L. Tognaccini, B.D. Howes, F. Sinibaldi, M.C. Piro, M. Fittipaldi, M.C. Baratto, R. Pogni, R. Santucci, G. Smulevich. Unravelling the non-native low-spin state of the cytochrome *c*−cardiolipin complex: evidence of the formation of a His-ligated species only, Biochemistry 56 (2017) 1887–1898.

[74] A. Paradisi, M. Bellei, L. Paltrinieri, C.A. Bortolotti, G. Di Rocco, A. Ranieri, M. Borsari, M. Sola, G. Battistuzzi. Binding of *S. cerevisiae* iso-1 cytochrome *c* and its surface lysine-to-alanine variants to cardiolipin: charge effects and the role of the lipid to protein ratio, JBIC, J. Biol. Inorg. Chem. 25 (2020) 467-487.

[75] L.J. McClelland, T.-C. Mou, M.E. Jeakins-Cooley, S.R. Sprang, B.E. Bowler. Structure of a mitochondrial cytochrome *c* conformer competent for peroxidase activity, Proc. Natl. Acad. Sci. U.S.A. 111 (2014) 6648-6653.

[76] S.M. Nold, H. Lei, T.-C. Mou, B.E. Bowler. Effect of a K72A mutation on the structure, stability, dynamics and peroxidase activity of human cytochrome *c*, Biochemistry 56 (2017) 3358−3368.

[77] A. Ranieri, G. Battistuzzi, M. Borsari, C.A. Bortolotti, G. Di Rocco, S. Monari, M. Sola. A bis-histidine-ligated unfolded cytochrome c immobilized on anionic SAM shows pseudo-peroxidase activity, Electrochem. Commun. 14 (2012) 29-31.

[78] Z. Wang, T. Matsuo, S. Nagao, S. Hirota. Peroxidase activity enhancement of horse cytochrome *c* by dimerization, Org. Biomol. Chem. 9 (2011) 4766-4769.

[79] P.P. Parui, Y. Sarakar, R. Majumder, S. Das, H. Yang, K. Yasuhara, S. Hirota. Determination of proton concentration at cardiolipin-containing membrane interfaces and its relation with the peroxidase activity of cytochrome c, Chem. Sci. 10 (2019) 9140-9151.

[80] B. Rieger, T. Arroum, M.-T. Borowski, J. Villalta, K.B. Busch. Mitochondrial F1FO ATP synthase determines the local proton motive force at cristae rims, EMBO Rep. 22 (2021) e52727.

[81] J. Babul, E. Stellwagen. The existence of heme-protein coordinate-covalent bonds in denaturing solvents, Biopolymers 10 (1971) 2359-2361.